



ELSEVIER

Contents lists available at ScienceDirect

## Graphical Models

journal homepage: [www.elsevier.com/locate/gmod](http://www.elsevier.com/locate/gmod)

## Direction-dependency of binary tomographic reconstruction algorithms

László Varga<sup>\*</sup>, Péter Balázs<sup>1</sup>, Antal Nagy<sup>1</sup>

Department of Image Processing and Computer Graphics, University of Szeged, Árpád tér 2, H-6720 Szeged, Hungary

## ARTICLE INFO

## Article history:

Received 20 August 2010

Received in revised form 21 June 2011

Accepted 22 June 2011

Available online xxxx

## Keywords:

Discrete tomography

Reconstruction

Non-destructive testing

Adaptive projection acquisition

GPU-accelerated computing

## ABSTRACT

In this work we study the relation between the quality of a binary tomographic reconstruction and the choice of angles of the projections. We conduct experiments on a set of software phantoms by reconstructing them from different projection sets using three different discrete tomography reconstruction algorithms, and compare the accuracy of the corresponding reconstructions with suitable approaches. To validate our results for possible real-world applications, we conduct the experiments by adding random noise of different characteristics to the simulated projection data, and by applying small topological changes on the phantom images as well. In addition, we also discuss some consequences of the angle-selection dependency and possible practical applications arising from the field of non-destructive testing, too.

© 2011 Elsevier Inc. All rights reserved.

## 1. Introduction

The basic problem of discrete tomography is to recover the structure of given objects from a set of their projections taken along specific directions. In the general case this problem can be solved, e.g., by the filtered backprojection method [1,2] that can reconstruct an object when a sufficiently large number of projections – usually a few hundreds – are available. However, in certain applications of tomography it is not possible to acquire so many projections.

*Discrete tomography* deals with the case when the objects to be reconstructed consist of only a few different materials, with known attenuation coefficients [3,4]. With this prior information, algorithms have been developed capable of producing acceptable reconstructions from only a few – usually 2–10 – projections. However, having so few projections defined by angles placed along the half circle

brings up new questions. Does the accuracy of the reconstructed results depend on how we choose these angles? If so, how should we choose the angles of the projections to obtain the best result possible for a given number of projections?

Such studies are motivated by practical applications. For example, in the non-destructive testing (NDT) of objects made of homogeneous materials, the acquisition of the projections may be very expensive. Therefore, it is important to keep the number of projections as small as possible. In NDT often a blueprint image is available, and the task is to determine how much a manufactured industrial part differs from the given blueprint. Usually, the object of interest might be placed with some rotation into the scanner, which may affect the accuracy of the reconstruction, and make the comparison to the blueprint impossible. If we assume that the projections of a given object are more informative from certain directions than from others we can use the blueprint image to determine how to put the objects into the scanner to get better results without making additional projections.

The aim of this paper is to determine – at least empirically – how dependent the discrete tomographic reconstructions can be, on the angles chosen for the projections. We do this by performing experimental tests on a set of software phantoms, trying to reconstruct them from different

<sup>\*</sup> Corresponding author. Fax: +36 62 546 397.

E-mail addresses: [vargalg@inf.u-szeged.hu](mailto:vargalg@inf.u-szeged.hu) (L. Varga), [pbalazs@inf.u-szeged.hu](mailto:pbalazs@inf.u-szeged.hu) (P. Balázs), [nagya@inf.u-szeged.hu](mailto:nagya@inf.u-szeged.hu) (A. Nagy).

<sup>1</sup> This research was in part supported by the TÁMOP-4.2.2/08/1/2008-0008 program of the Hungarian National Development Agency and by the TÁMOP-4.2.1/B-09/1/KONV-2010-0005 Project co-financed by the European Union and the European Regional Development Fund. The work of the second author was also supported by the János Bolyai Research Scholarship of the Hungarian Academy of Sciences.

projection sets. This paper is an extended version of the conference article [5] and it extends the previous studies by experimenting on two additional binary tomography reconstruction algorithms, and also the case when the measured projection data is affected by noise, or the object to be reconstructed is somehow distorted.

The paper is structured as follows. In Section 2 we start out by introducing the continuous and discrete reconstruction problems and some basic approaches for solving them. In Section 3 we describe three different algorithms for binary tomography used in our experiments. In Section 4 we provide a detailed explanation of the experiments we conducted and in Section 5 we discuss the results and their interpretation. In Section 6 we propose a possible application of our results in the field of non-destructive testing and finally, in Section 7 we conclude the results and highlight the possible extensions of our work.

## 2. The reconstruction problem

We examine the case of two-dimensional transmission tomography with parallel beam geometry which is a general and widely studied problem. The mathematical formulation of this task can be given as follows.

There is a given  $f : \mathbb{R}^2 \rightarrow \mathbb{R}$  function (which represents e.g. a 2-dimensional cross-section of a real world object). Although the function  $f$  itself is considered to be unknown, we can produce its projections given by a set of its line integrals determined by the Radon-transform [1,2] as

$$[\mathcal{R}f](\alpha, t) = \int_{-\infty}^{\infty} f(t \cos(\alpha) - q \sin(\alpha), t \sin(\alpha) + q \cos(\alpha)) dq. \quad (1)$$

In the above formulation the  $\alpha$  and  $t$  values, respectively, describe the direction and the position of a line with its points parameterized by  $q$ . The task of tomographic reconstruction is to find an  $f' : \mathbb{R}^2 \rightarrow \mathbb{R}$  function that satisfies  $[\mathcal{R}f](\alpha, t) = [\mathcal{R}f'](\alpha, t)$  for a set of predetermined  $(\alpha, t)$  pairs, i.e., which has the same projections as the unknown  $f$  function in a specific set of directions.

In the ideal case when every  $[\mathcal{R}f](\alpha, t)$  values are available for all  $\alpha \in [0^\circ, 180^\circ)$  and  $t \in \mathbb{R}$  values, the above task can easily be done by exact mathematical methods [1]. Unfortunately, in real applications it is impossible to handle an infinite number of values, therefore we usually have to add a few restrictions to the model.

In the sequel we will assume that the function to be reconstructed is binary (i.e.,  $f : \mathbb{R}^2 \rightarrow \{0, 1\}$ ), has a bounded support and has constant values over each unit square shaped areas defined by the 2-dimensional rectangular grid. More formally we can say that

$$f(u+a, v+b) = f(u+c, v+d) \quad \forall u, v \in \mathbb{Z} \quad \forall a, b, c, d \in [0, 1). \quad (2)$$

In this way the problem can be regarded as the reconstruction of an  $n \times n$  sized binary image from its projections. In addition, we will further assume that each projection consists of a finite number of projection lines where the distance between the consecutive lines is always unitary. More exactly, for each  $t$  value in (1)

$$t \in \left\{ k + 1/2 \mid k \in \mathbb{Z}, |k + 1/2| < n/\sqrt{2} \right\}, \quad (3)$$

assuming that the origin is placed onto the center of the image.

Using this discretized model, the binary reconstruction problem can be represented as a system of equations

$$\mathbf{Ax} = \mathbf{b}, \quad \mathbf{A} \in \mathbb{R}^{n^2 \times m}, \quad \mathbf{x} \in \{0, 1\}^{n^2}, \quad \mathbf{b} \in \mathbb{R}^m, \quad (4)$$

where

- $\mathbf{x}$  is the vector of all  $n^2$  unknown image pixels,
- $m$  is the total number of projection lines used,
- $\mathbf{b}$  is the vector of all  $m$  measured projection values,
- $\mathbf{A}$  describes the projection geometry with all  $a_{i,j}$  elements giving the length of the line segment of the  $i$ th projection line through the  $j$ th pixel

as illustrated in Fig. 1.

Although (4) gives an exact formulation of the reconstruction problem, a direct approach for solving the related equation system is usually not the best strategy. As mentioned before, in discrete tomography just a handful of projections are available, therefore the corresponding system of equations is usually underdetermined, and – due to errors in the measured projection data – it can be inconsistent as well. There are two main approaches to overcome these problems. First, one can apply iterative algorithms for finding an approximate solution. These methods are the different versions of the so-called algebraic reconstruction technique [1,2,6]. The other main approach is based on defining an energy function

$$\mathcal{C}(\mathbf{x}) = \|\mathbf{Ax} - \mathbf{b}\|_2^2 + \lambda \cdot g(\mathbf{x}), \quad (5)$$

where  $\mathbf{A}$ ,  $\mathbf{b}$ , and  $\mathbf{x}$  are the same as defined in (4) and  $g(\mathbf{x})$  is a function representing prior information about the image to be reconstructed, with a given  $\lambda$  weight. After this reformulation, the reconstruction problem can be solved by finding the minima of the function  $\mathcal{C}(\mathbf{x})$  with some optimization strategies, like genetic algorithms, simulated annealing, or other numerical methods [4,7–10].

## 3. Applied reconstruction algorithms

We examine the behavior of three different discrete tomographic reconstruction algorithms. All of them are fast, deterministic methods, suitable for parallel implementation on modern hardware. In the sequel we will give a brief introduction of these algorithms.

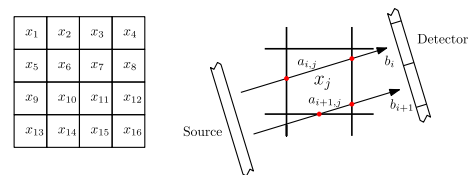


Fig. 1. Representation of the ordering of the pixels and the parallel beam geometry.

### 3.1. Thresholded Simultaneous Iterative Reconstruction Technique (TSIRT)

The TSIRT algorithm performs a continuous reconstruction followed by a thresholding. In our case the continuous reconstruction is produced by the Simultaneous Iterative Reconstruction Technique (SIRT) [1,2], which is an iterative algorithm for finding an approximate solution of (4). After obtaining the continuous result we simply apply a thresholding with a 0.5 threshold value in order to get a binary solution.

### 3.2. Discrete algebraic reconstruction technique

The second algorithm is the Discrete Algebraic Reconstruction Technique (DART) [6], which is an iterated thresholding of continuous reconstructions. This algorithm starts out by producing a continuous reconstruction using an algebraic reconstruction method. Then, in each iteration it applies a thresholding on the continuous result, and proceeds with another continuous reconstruction, performed only on the boundary of the thresholded image.

In our experiments the continuous reconstructions consisted of 10 iterations of the SIRT algorithm, and the threshold was set uniformly to 0.5.

### 3.3. Energy minimization tomography by DC programming

The third algorithm (that was first introduced in [9]) applies DC programming (a numerical method for minimizing the difference of convex functions), to minimize a sequence of energy functions given as

$$\mathcal{J}_\lambda(\mathbf{x}) := \|\mathbf{Ax} - \mathbf{b}\|_2^2 + \frac{\gamma}{2} \sum_{j=1}^{n^2} \sum_{l \in N_4(j)} (x_j - x_l)^2 - \lambda \frac{1}{2} \langle \mathbf{x}, \mathbf{x} - \mathbf{e} \rangle,$$

$$\mathbf{x} \in [0, 1]^{n^2}. \quad (6)$$

Here  $\gamma$  is a given constant controlling the weight of the smoothness term on the image,  $N_4(j)$  is the set of pixels 4-connected to the  $j$ th pixel, and  $\mathbf{e}$  denotes the vector with all  $n^2$  coordinates equal to 1. In the beginning of the optimization process  $\lambda = 0$ , so the best continuous solution is found. In the sequel,  $\lambda$  is iteratively increased by  $\lambda_\Delta$ , to force binary results. From this point we will simply call this algorithm “DC”.

During the reconstructions the parameters of the DC algorithm were mostly set as specified in [10], for example we used  $\gamma = 0.25$ . Though, instead of calculating  $\lambda_\Delta$  from the first continuous reconstruction and the projection matrix  $\mathbf{A}$ , we explicitly set it to  $\lambda_\Delta = 0.1$ , to avoid performing a large number of computation, and keep the running time of the algorithm as low as possible.

## 4. Test data and experiment settings

We conducted several experiments on binary software phantoms, reconstructing them with different reconstruction algorithms under different conditions, and evaluated the results with various approaches. In this chapter we

give a thorough description of our test frameset, and introduce the numerical tools we used for analyzing the data.

### 4.1. Test dataset

The core of our image database consisted of 22 phantoms, but for simulating small topological changes present on the object of study in real-world applications (i.e., bubbles or fractures) we also produced a slightly altered version of all the images, too. All the phantoms had the same size of 256 by 256 pixels. Some of the phantoms of our test database can be seen in Fig. 2 and one example for the altered images is given in Fig. 3.

For simulating measurement errors during the projection acquisition phase of a real-world application, some of the experiments were performed using projection data corrupted by noise. In a real application the gathered projection data can be degraded by different artifacts – e.g., beam hardening, photon scattering, imperfections of the detectors, background noise, etc. – most of which can be handled by preprocessing steps [11–14]. Unfortunately, it was impossible to simulate all these effects in our experiments. Therefore, we decided to restrict our studies to an additive Gaussian background noise, which is a common technique for modeling noise in transmission tomography [10,13–15].

In each case the mean value of the noise was set to  $\mu = 0$ , and the standard deviation was chosen from the set  $\sigma \in \{0.5; 1.5; 5.0\}$ . With the specified noise we performed each reconstruction four times – once without changing the projection data and three times using the three different levels of additive noise. We generated the noise beforehand, and stored it in a file, therefore we could use the same noise for all reconstructions.

### 4.2. Applied projection geometries

The reconstructions of the test objects were performed from projection sets with different numbers of projection. Each time the projection angle sets were chosen equiangularly on the half circle. In this way an angle set is uniquely determined by its number of projections  $p$  and a starting angle  $\alpha$  as

$$S(\alpha, p) = \left\{ 90^\circ + \alpha + i \frac{180^\circ}{p} \mid i = 0, \dots, p-1 \right\}. \quad (7)$$

Fig. 4 gives an example using 4 projections.

For each image the number of projections  $p$  ranged from 2 to 16, and for each such projection set the starting angle  $\alpha$  varied from  $0^\circ$  to  $\left(\left\lceil \frac{180}{p} \right\rceil - 1\right)^\circ$  with a step of  $1^\circ$ . An illustration of the different projection sets can be seen in Fig. 5. This makes a total of  $\sum_{i=2}^{16} \left\lceil \frac{180}{i} \right\rceil = 431$  different reconstruction tasks for each image and noise level.

### 4.3. Implementation

The reconstruction algorithms were implemented with GPU acceleration using the NVIDIA CUDA programming toolkit [16]. For the computation we used a 2.66 GHz Core 2 Quad CPU, and an NVIDIA GeForce GTS250 GPU. With

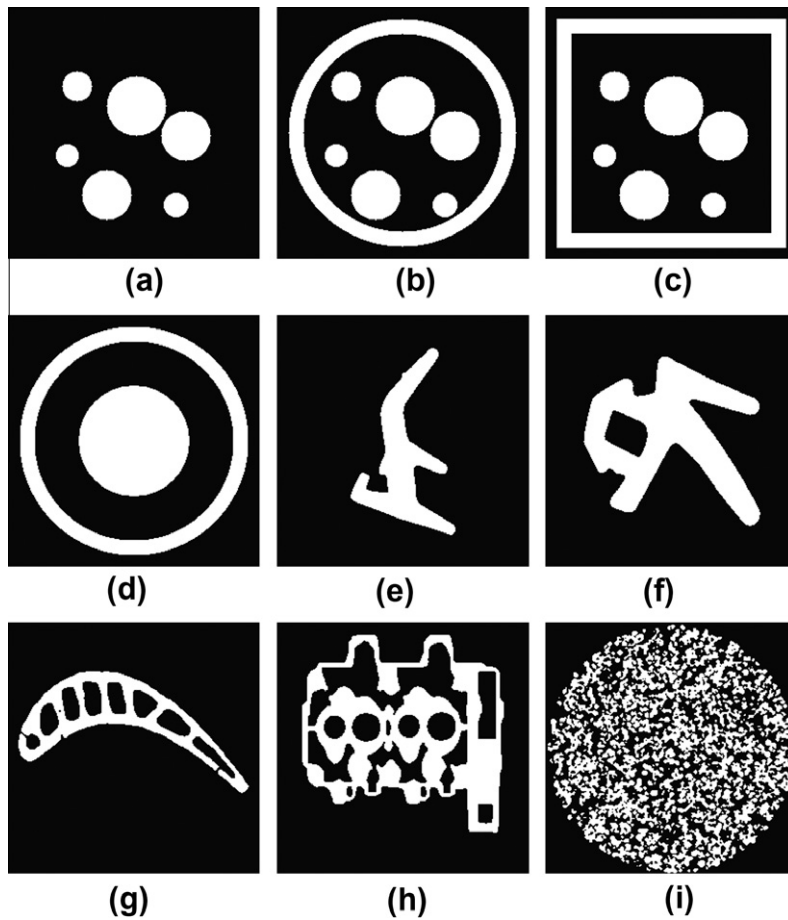


Fig. 2. Some of the software phantoms used for testing.

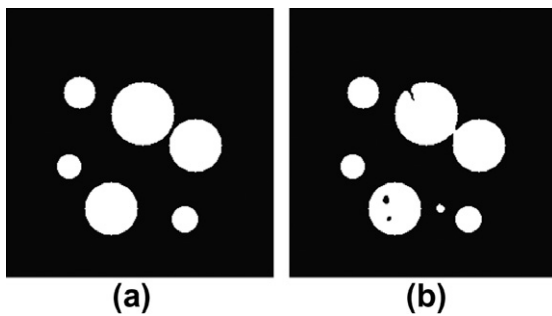


Fig. 3. Sample of the modifications in the phantoms with the original (a), and the altered image (b).

this highly parallel implementation the time required to perform all the 227,568 reconstruction tasks (2 versions of 22 phantoms reconstructed from 431 projection sets affected by 4 different levels of noise with 3 reconstruction algorithms) was about 100 h.

#### 4.4. Numerical tools for comparison

After performing the reconstructions we compared the results by measuring the accuracy of the reconstructed

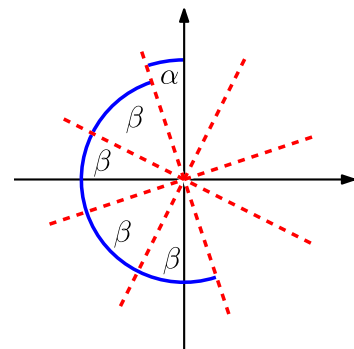
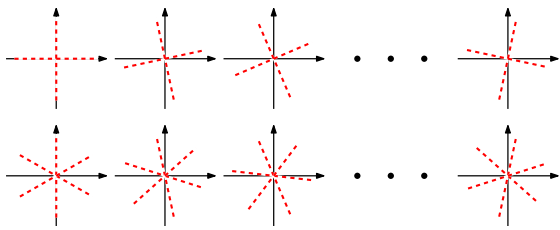


Fig. 4. The projection sets  $S(\alpha, 4)$  used in the tests ( $\alpha$  is predefined,  $\beta = 45^\circ$ ).

images. For the purpose of error measurement we used the Relative Mean Error (RME) values of the reconstructions given as

$$RME(\mathbf{x}^*, \mathbf{y}) = \frac{\sum_{i=1}^{n^2} |x_i^* - y_i|}{\sum_{i=1}^{n^2} (x_i^*)}. \quad (8)$$

In the above formulation  $\mathbf{x}^*$  stands for the vector of the pixel values on the expected reconstruction result, and  $\mathbf{y}$  denotes an arbitrary reconstruction. Assuming that the



**Fig. 5.** The projection sets used for testing the reconstruction algorithms with 2 (top row) and 3 (bottom row) projections. Dashed red lines represent the direction of the projections. (For interpretation of the references to color in this figure legend, the reader is referred to the web version of this article.)

original and the reconstructed images are binary the *RME* value gives the number of misreconstructed pixels on the result normalized by the number of object pixels on the expected reconstruction. Note that the *RME* value can be greater than 1, since it depends on the number of object pixels of an image.

We also needed an exact numeric evaluation of the direction-dependency of the results. With the aid of such a measurement we could compare the direction-dependencies of different phantoms, reconstruction algorithms and numbers of projections. In the same time, it was also useful for finding the images more dependent to rotation, therefore we could concentrate on the more relevant parts of the results. For this purpose we came up with a suitable function. Before giving the exact specification we also need to introduce some notations.

In the sequel  $\mathbf{R}_{Alg}(\mathbf{x}^*, p, \alpha)$  will denote the reconstruction of the  $\mathbf{x}^*$  expected image from the projection set determined by the angles of  $S(\alpha, p)$ , reconstructed by a given *Alg* reconstruction algorithm described in Section 3. For example  $\mathbf{R}_{DC}(\mathbf{x}^*, 4, 0^\circ)$  denotes the reconstruction of an  $\mathbf{x}^*$  phantom performed with the DC algorithm using the projection set containing 4 equiangular projections with a  $0^\circ$  starting angle. After this, let

$$\mathbf{R}_{Alg}(\mathbf{x}^*, p) := \left\{ \mathbf{R}_{Alg}(\mathbf{x}^*, p, \alpha) \mid \alpha = 0, \dots, \left( \left\lceil \frac{180}{p} \right\rceil - 1 \right)^\circ \right\} \quad (9)$$

be the set of all reconstructions of the same phantom, performed with the same reconstruction algorithm, always from the same number of projections but with all possible starting angles.

With the previous notations our direction-dependency measurement can be given as

$$D_{Alg}^\sigma(\mathbf{x}^*, p) := \left( E_{Alg}^{\max}(\mathbf{x}^*, p) - E_{Alg}^{\min}(\mathbf{x}^*, p) \right) \cdot \exp \left( - \frac{(E_{Alg}^{\min}(\mathbf{x}^*, p))^2}{\sigma^2} \right), \quad (10)$$

where

$$E_{Alg}^{\min}(\mathbf{x}^*, p) := \min \{ RME(\mathbf{x}^*, \mathbf{y}) \mid \mathbf{y} \in \mathbf{R}_{Alg}(\mathbf{x}^*, p) \}, \quad (11)$$

and

$$E_{Alg}^{\max}(\mathbf{x}^*, p) := \max \{ RME(\mathbf{x}^*, \mathbf{y}) \mid \mathbf{y} \in \mathbf{R}_{Alg}(\mathbf{x}^*, p) \}. \quad (12)$$

The function in (10) simply determines the highest difference in the *RME* values of the corresponding results and

multiplies it with a correction function. With the aid of this correction function we can set a  $\sigma$  approximate upper threshold of the *RME* we are interested in. Having this direction-dependency measurement, a higher value means that the quality of the reconstruction is more dependent on the choice of the directions for a specific number of projections.

## 5. Experimental results

In this section we present the results of the experimental tests and provide some explanation of them. Unfortunately, the extremely large number of the performed reconstructions makes it impossible to give all the results. Therefore, we will only collect our most important observations and supply samples of the results for supporting them. The full database of all the numerical results is available on the web [17].

Since this paper is an extension of our previous work [5] – that only used the DC algorithm for the experiments – we first discover the basic tendencies in the results of the DC algorithm concentrating on the case when the data was not corrupted by any noise or other changes. We will discuss the results of the other reconstruction algorithms and the effects of the modifications on the data later on in this chapter.

We used the function of (10) to find the reconstruction setups which are the most sensitive to rotation. Of course, in a real application only accurate reconstructions are acceptable, so we were interested in the cases when the results had only small errors. For this purpose we set  $\sigma = 0.05$  in (10). Fig. 6 shows the values of our direction-dependency measurement  $D_{DC}^{0.05}(\mathbf{x}^*, p)$  for Fig. 2a–c which are the three different versions of the same basic phantom.

First, let us take a look at the curves belonging to the phantom of Fig. 2a, i.e., the basic phantom, that has no ring or rectangular stripe around the disks. We can observe the two higher values in the case of four and five projections that suggest that the reconstruction of this phantom is the most dependent on the rotation of the projection set when four or five projections are available. This can be explained by examining the minimal and maximal *RME* values of the corresponding reconstructions according to the number of projections.

In Fig. 7a the curves belonging to the minimal and maximal errors are descending simultaneously as the number of projections increases. This tendency is obvious, since having more projections means more information which yields better reconstructions. It is also important to notice, that the curves belonging to the minimal *RME*s reach an almost zero value with a smaller number of projections than the maximal *RME*s. Since, we designed our direction-dependency measurement for finding such differences (where a significant improvement of the reconstructed result can be reached by finding the appropriate projection angles), this is where it shows higher values.

In fact, we could deduce something similar for most of the phantoms and reconstruction algorithms. The overall tendency shows that the direction-dependency of the images in our database is notably higher for only a few numbers of projections. In practice this means that at those specific projection numbers we can obtain entirely differ-

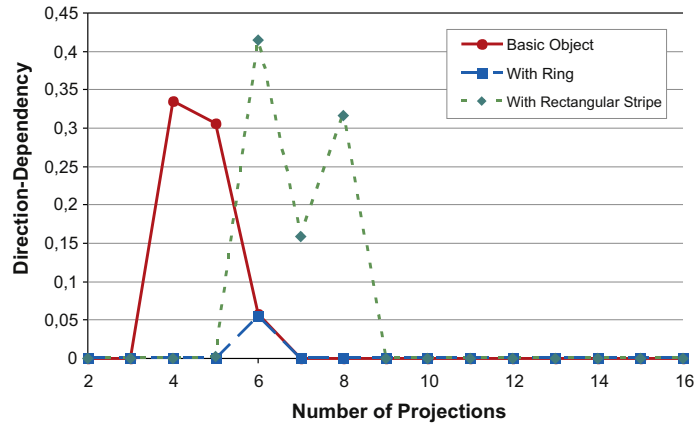


**Fig. 6.** Direction-dependency of the software phantoms of Fig. 2a–c (the higher the values are the more dependent the projection setup is to the choice of directions).

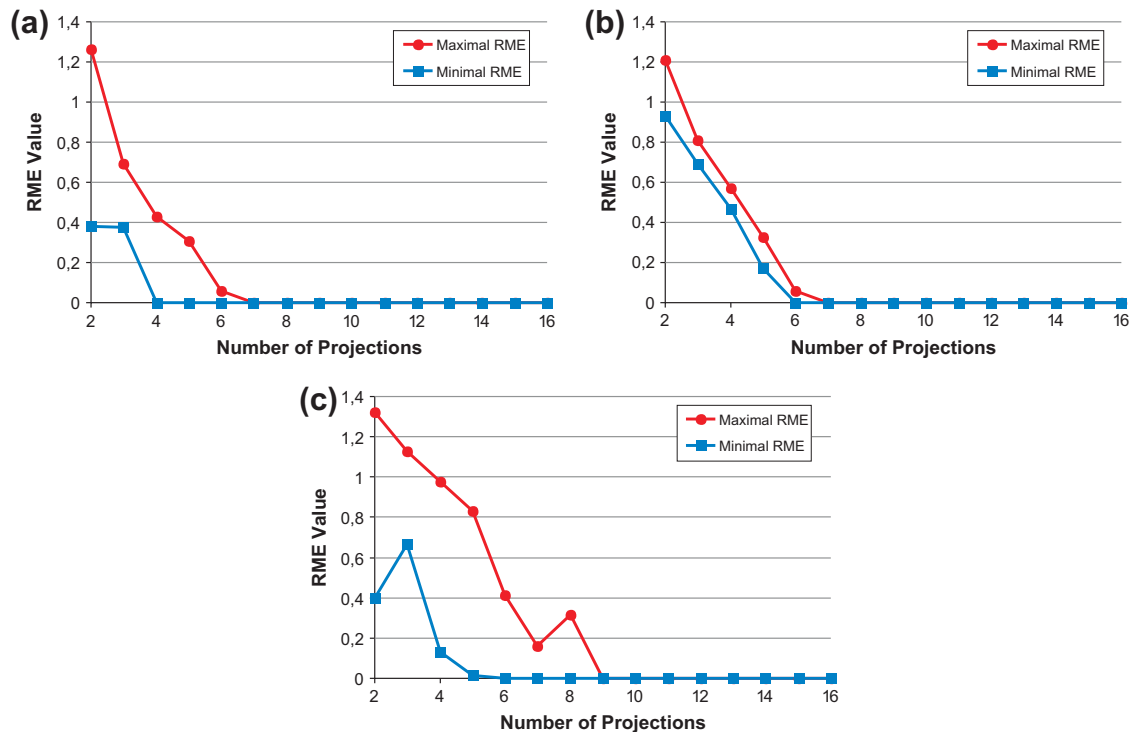


**Fig. 7.** Minimal and maximal RME values as they depend on the number of projections, for the software phantom of Fig. 2a: (a), Fig. 2b: (b) and Fig. 2c: (c).

ent reconstructions of the same objects only by picking different projection angles. Examples of such differences in the reconstructions can be seen in Fig. 8.

It is also useful to study the reconstructions belonging to the angles between the extremas. Plotting the RME values can provide valuable information about that. Fig. 9 shows the graph of RME values of the  $\mathbf{R}_{DC}(\mathbf{x}^*, 4)$  sets belonging to the phantoms of Fig. 2a–c and the  $\mathbf{R}_{DC}(\mathbf{x}^*, 2)$  sets belonging to Fig. 2d. As we can see, the curves of Fig. 9 are relatively smooth. This indicates that projections with angles close to each other have similar information content. This can lead to interesting consequences. First,

we can say that equiangular projection sets, having similar  $\alpha$  starting angles would probably produce similar reconstructions. On the other hand, we are convinced that there is no use of an angle step less than  $1^\circ$  in the experiments. Another consequence that fits to our overall observations is that the direction-dependency of the reconstructions reduces when we increase the number of projections. Therefore, significant differences between the best and worst reconstructions can only be expected when only a few projections are available. This also means that more complex objects – requiring more projections for a proper reconstruction – are less dependent on the choice of angles.

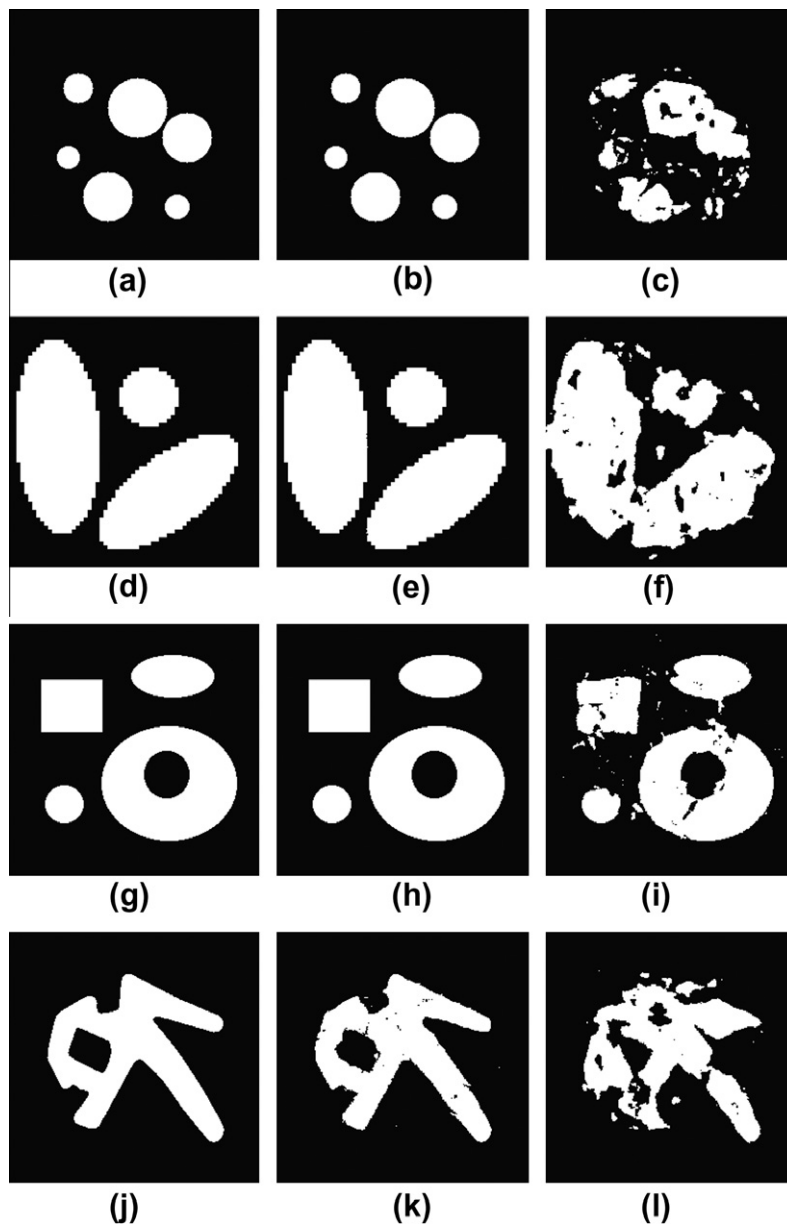


**Fig. 8.** Examples for the best and worst reconstructions of software phantoms, produced by the DC algorithm, with given projection numbers. The original phantoms (first column), and the best and worst results (second and third column, respectively) for the same number of projections but different starting angles.

As it was mentioned above, we used different types of phantom images, some of which were created for specific reasons. For example the phantoms on Fig. 2a–c are the three different versions of the same phantom – a basic one with only six disks on it, one with a ring and one with a rectangular stripe around the disks. We can see (on the left hand side of Fig. 9) that the reconstruction is the best when there is nothing around the disks.

If we add a rectangular stripe to the phantom the whole characteristic of the curve changes (see again Fig. 9). In this case the *RME* values are the smallest when the starting angle of the projection set is close to  $0^\circ$ . With the proper projections – when two angles are aligned to the sides of the

rectangle – the rectangular stripe can be perfectly reconstructed and it does not affect the quality of the reconstruction. Furthermore, the farther the projection angles are from the proper alignment, the less accurate the reconstruction is. This means that adding such – highly angle-dependent – objects to a phantom can greatly increase the direction-dependency of the reconstructions. This is also the reason why we can see larger differences between the curves of Fig. 7c, and higher values of the direction-dependency measurement in Fig. 6.

The effect is entirely different if we add a ring to the phantom. In the ideal case a ring is rotation invariant and affects all the possible projections in the same way. In

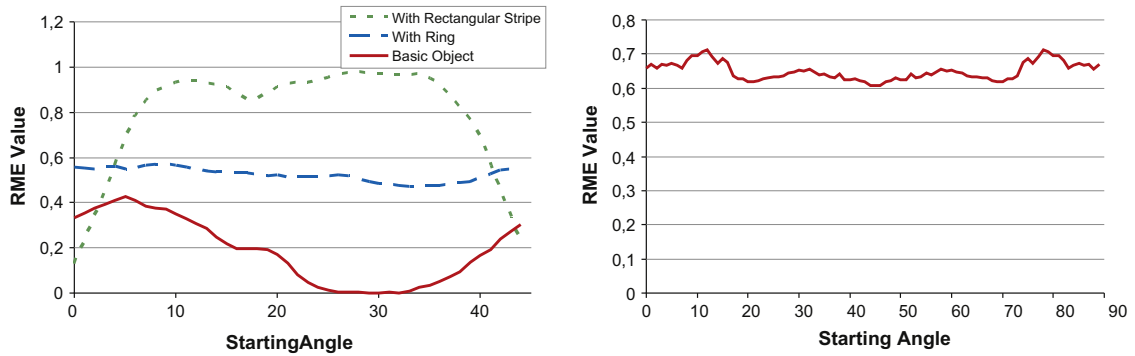


**Fig. 9.** Example for the RME values, for the software phantoms of Fig. 2a–c reconstructed from 4 projections (left) and Fig. 2d reconstructed from 2 projections (right).

Fig. 9 this results in a shifting of the RME values of the original curve with all the reconstructions getting worse, but the basic curvature is still similar. Our guess is that adding such a rotation invariant object to the phantom brings more instability into the equation system describing the reconstruction problem and thus makes it harder to produce accurate results. This also means that the minimal and maximal values on Fig. 7b are relatively close to each other and hence the direction-dependency of the reconstructions is smaller (as it is shown in Fig. 6).

Another case worth examining is when the whole phantom is constructed to be rotation invariant. The phantom of Fig. 2d is composed of only one disk and a ring. We would expect this phantom to be rotation independent, i.e., to have the same reconstructions from any equiangular projection sets. Surprisingly, this is not the case. We have given the RME values for this phantom produced from 2 projections with the DC algorithm according to the starting angle in the right hand side of Fig. 9. We can see that even this phantom has some degree of direction-dependency. The reason for this symptom can be found in the representation used for the reconstruction. As we mentioned before, we assumed that the object to be reconstructed is represented on the two dimensional integer lattice and the phantoms were given as binary images. We are convinced that the pixelization can also have a serious affect on the reconstructions, but investigating the problems caused by the discretization is out of the scope of our present work.

Now, let us consider the results belonging to the different reconstruction algorithms and to the different types of modified data. For this purpose, Fig. 10 shows the RME values of the different reconstructions of the phantoms of Fig. 3 produced from four projections, but by different reconstruction algorithms and with different types of noise on the measured projection data. We can see that all the curves show some degree of similarity i.e. the minimal and maximal values are determined by the same projection sets. This indicates that no matter if we use different reconstruction algorithms, or the data is corrupted by noise, always the same projections will contain more information for the reconstruction than other ones. Even if the object to be reconstructed is somehow distorted, the information content of the projections will not change considerably, as long as the modifications affect only small parts of the object.

After comparing hundreds of similar diagrams we can state that all the observations discussed above remain consistent with other reconstruction algorithms, slightly altered images and with noisy projections as well.

Finally, it is also useful to compare the direction-dependencies of the three reconstruction algorithms, as it is shown in Fig. 11 for some of the phantoms used in our studies, according to the number of projections. The first thing to note is that some of the phantoms are less dependent on the choice of angles, regardless of the reconstruction algorithm used. As we mentioned above, more complex objects, requiring more projections for an acceptable reconstruction, are less dependent on the choice of angles, since in these cases the high number of projections reduce the freedom of choosing directions.

When comparing the curves in each subfigure, we can see that – apart from small differences – the curves belonging to the DC and DART algorithms are alike, i.e., the local maxima are close to each other, and the corresponding values are almost equal. These similarities arise from the fact, that both algorithms use the same prior information in their reconstruction (the fact that we are looking for somewhat smooth, binary results), therefore their results are close to each other.

The case is different when we examine the curves belonging to the TSIRT algorithm. Since this algorithm is not more complex than a continuous reconstruction it provides poor results, and thus it requires several projections for a highly accurate reconstruction. Here, the high number of required projections, again, reduces the freedom of choosing projection angles and suppresses the direction-dependency. This also means that one can reduce the effects of direction-dependency by using less accurate reconstruction algorithms and more projections, but this approach would be against our goal of gaining more accurate results while reducing the number of required projections.

## 6. Direction-dependency in the field of non-destructive testing

In industry, there is often a need to get information about the interior of objects (industrial parts) in a non-destructive way, i.e. without damaging the object itself. This process is called non-destructive testing (NDT). In these applications the information about the object is usu-

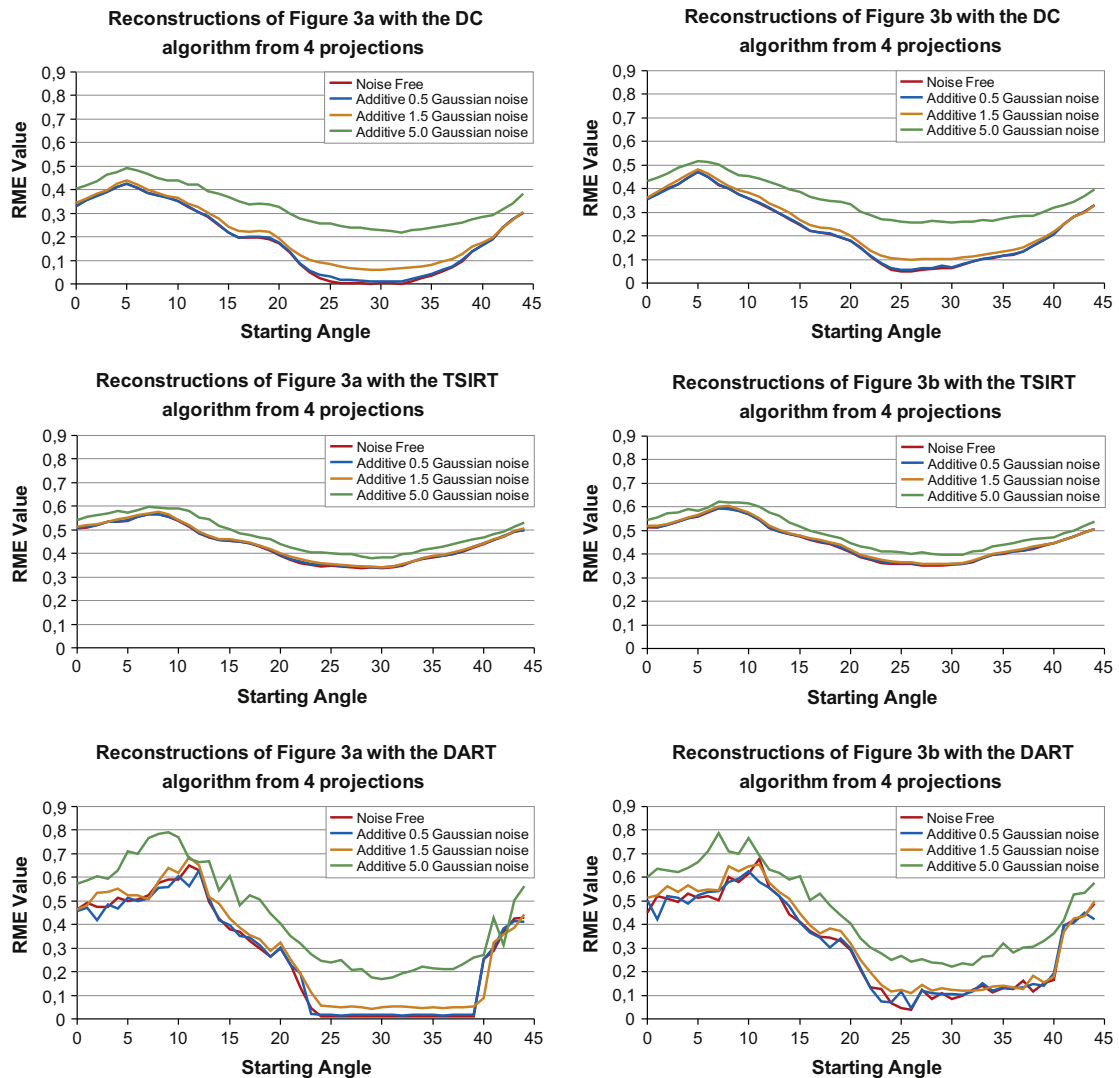


**Fig. 10.** RME values of the reconstructions of the phantoms of Fig. 3 from 4 projections according to the starting angle. The diagrams on the left hand side are the reconstructions of Fig. 3a, and those on the right hand side are the reconstructions of Fig. 3b. Each row shows the results of one applied reconstruction algorithm (in order from the top to the bottom: DC, TSIRT and DART algorithms). Each diagram contains four curves belonging to the reconstructions affected by the four different types of noise.

ally collected by transmission tomography using X-rays or neutron rays to form the projections of the object. Since the acquisition of such projections can be very expensive and time-consuming, it is important to keep the number of projections as small as possible. If the object is made of homogeneous material then one approach to achieve this is to apply binary tomography for the reconstruction [11,12].

A frequent task in NDT is to determine the differences between the studied object and a given blueprint image. One places the object into the scanner, forms its projections from a few directions, and applies a (binary) reconstruction method to obtain an image from the object. Finally, the difference of the blueprint and the reconstructed images is measured according to an arbitrary similarity metric. Since the blueprint image is available

in advance, we can simulate its projections in arbitrary directions, and perform all the tests of Section 5 in order to characterize the blueprint image from the viewpoint of direction-dependency. This information turns out to be essentially useful in several scenarios of NDT.

If there is a reference mark on both the benchmark and the studied objects then it is possible to place this latter one with a rotation of arbitrary degree into the scanner. From the dependency function of the blueprint image, similar to that of Fig. 9, we know when the best reconstruction quality can be achieved – we simply have to seek the global minimum of the function. This determines how (i.e., in which direction) to place the test object into the scanner to have the most accurate reconstruction from the available number of projections. Since the translation between RME values is smooth, it is sufficient to

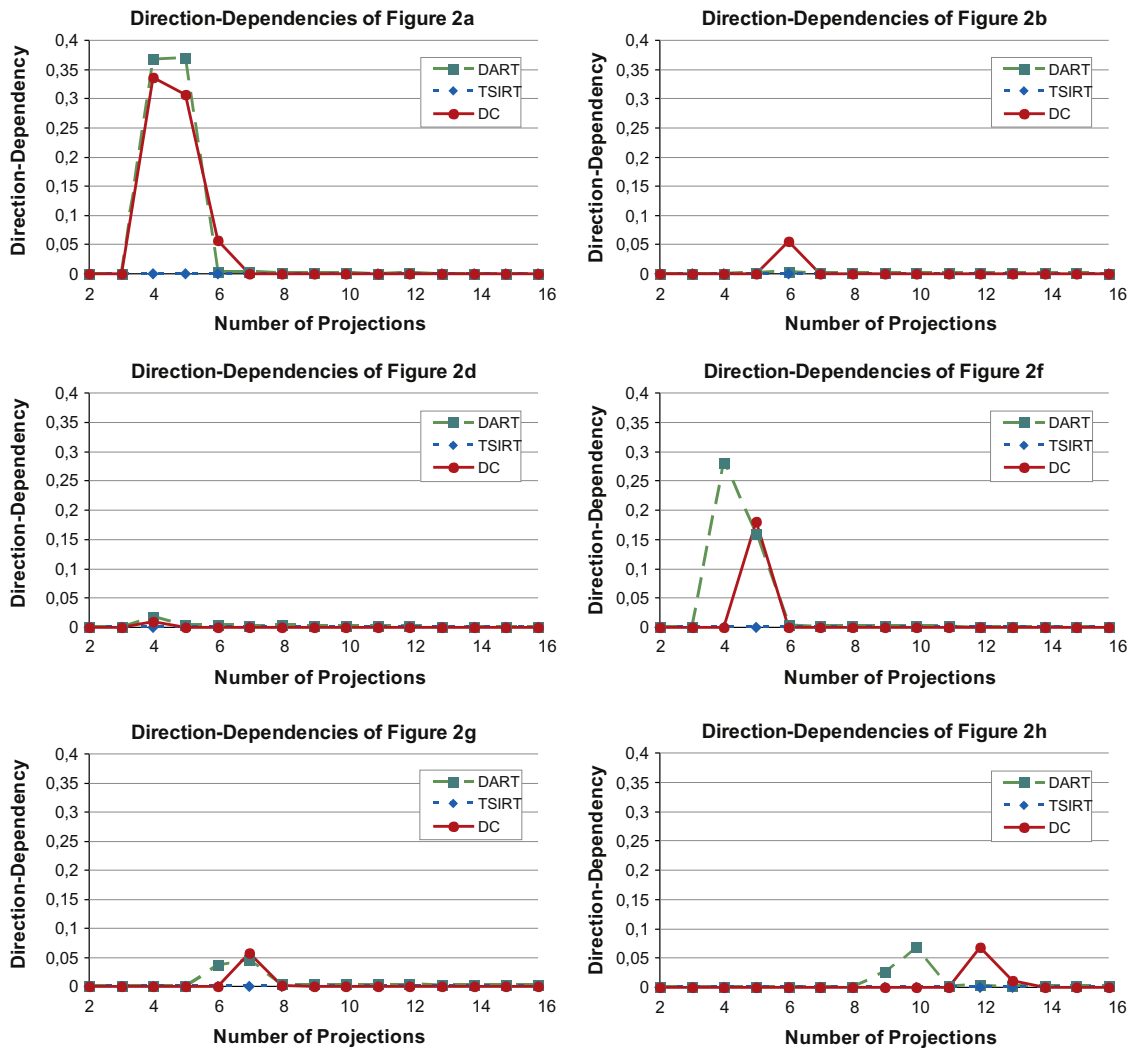


**Fig. 11.** Direction-dependencies of the different reconstruction algorithms, on some of the phantoms used in our work. Each subfigure contains the direction-dependencies ( $D_{Alg}^{0.05}(\mathbf{x}^*, p)$  values described in Section 4) of the reconstruction algorithms, on a specific phantom image, according to the number of projections.

place the object with only approximately the same rotation as the minimal *RME* value suggests. (For more sophisticated projection angle selection algorithms see [18].)

On the other hand, if there is no mark on the studied object, then it might be placed with an unknown rotation into the scanner. Again, from the dependency function of the blueprint image we can predict how sensitive our test will be to this rotation. In addition, from the graph of the blueprint image similar to that of Fig. 7 we can deduce how many projections are needed to keep the maximal error acceptably low, i.e., to be sure that the effect of rotation will be eliminated. If it is impossible to acquire so many projections, then from the minimal error we can estimate the best reconstruction possible from the given number of projections. This information can also be used to check whether a reconstruction algorithm is suitable for the given industrial test. If the error of the best reconstruction is still high, then we might classify perfect objects as damaged ones and vice versa.

## 7. Conclusion and further work

The aim of this paper was to study how the accuracy of binary tomography algorithms depend on the directions of the projections available for the reconstruction. We conducted experimental software test on a set of phantom images and compared the results from different points of view. We found that certain objects behave considerably sensitively from the viewpoint of direction-dependency. On the other hand, there are objects for which the result of the reconstruction is less dependent on the direction of the projections, but even in those cases choosing the proper directions can reduce the number of projections needed for an accurate reconstruction. Our investigations can be essentially useful in the non-destructive testing of industrial objects made of homogeneous materials.

Our results are general in the sense that they represent experiments performed on a large dataset. We performed reconstructions on various types of binary images recon-

structed by three different reconstruction algorithms from several different projection sets. We also studied the case when the object to be reconstructed undergoes slight topological changes or the measured projection data is affected by random noise of different characteristics, too.

The presented results can be extended in many different ways. In our future work we intend to examine whether the observations of this paper still hold if the projections are non-equiaxially acquired, the investigated objects consist of more than one materials or in the case of three-dimensional reconstructions. In addition, we are also planning to extend the studies to real-world applications.

Our results suggest that there is a deeper theoretical explanation of our observations, laying in the background. We think that finding a connection between the theory and our experimental results would be a major breakthrough. The desire for such theory is not unfamiliar in discrete tomography. Explanations have already been published for special cases of the problem [3,4,19–21], and the authors of [22] have also suggested the examination of empty-, and full-lines (i.e., when projection values are close to their reachable minimum or maximum) for determining the information content of different projections. However, to our knowledge there is no thorough explanation of the general case so far.

Finally, we are also planning to extend our studies to adaptive projection acquisition (like in [23]), i.e., determining the best directions for the projections during the data acquisition, by using information gathered from the previously made projections.

## Acknowledgments

The authors would like to thank Joost Batenburg and Christoph Schnörr for providing test images to the studies and highlight that another set of phantoms were taken from the image database of the IAPR Technical Committee on Discrete Geometry (TC18). We are also grateful to David Ress for suggesting the usage of small topological modifications on the test images, and to the reviewers for their valuable comments.

## References

- [1] A.C. Kak, M. Slaney, Principles of Computerized Tomographic Imaging, IEEE Press, New York, 1999.
- [2] G.T. Herman, Fundamentals of Computerized Tomography, Image Reconstruction from Projections, second ed., Springer-Verlag, London, 2009.
- [3] G.T. Herman, A. Kuba (Eds.), Discrete Tomography: Foundations, Algorithms and Applications, Birkhäuser, Boston, 1999.

- [4] G.T. Herman, A. Kuba (Eds.), Advances in Discrete Tomography and Its Applications, Birkhäuser, Boston, 2007.
- [5] L. Varga, P. Balázs, A. Nagy, Direction-dependency of a binary tomographic reconstruction algorithm, Lecture Notes in Computer Science 6026 (2010) 242–253.
- [6] K.J. Batenburg, J. Sijbers, DART: a fast heuristic algebraic reconstruction algorithm for discrete tomography, IEEE Conference on Image Processing IV (2007) 133–136.
- [7] P. Balázs, M. Gara, An evolutionary approach for object-based image reconstruction using learnt priors, Lecture Notes in Computer Science 5575 (2009) 520–529.
- [8] V. Di Gesu, G. Lo Bosco, F. Millonzi, C. Valenti, A memetic algorithm for binary image reconstruction, Lecture Notes in Computer Science 4958 (2008) 384–395.
- [9] T. Schüle, C. Schnörr, S. Weber, J. Hornegger, Discrete tomography by convex-concave regularization and DC programming, Discrete Applied Mathematics 151 (2005) 229–243.
- [10] S. Weber, A. Nagy, T. Schüle, C. Schnörr, A. Kuba, A benchmark evaluation of large-scale optimization approaches to binary tomography, Lecture Notes in Computer Science 4245 (2006) 146–156.
- [11] S. Kimmel, J. Baumann, Z. Kiss, A. Kuba, A. Nagy, J. Stephan, Discrete tomography for reconstruction from limited view angles in non-destructive testing, Electronic Notes in Discrete Mathematics 20 (2005) 455–474.
- [12] J. Baumann, Z. Kiss, S. Krimmel, A. Kuba, A. Nagy, L. Rodek, B. Schillinger, J. Stephan, Discrete Tomography Methods for Nondestructive Testing (2007) 303–331 (Chapter 14 of [4]).
- [13] N.D.A. Mascarenhas, C.A.N. Santos, P.E. Cruvinel, Transmission tomography under Poisson noise using the Anscombe transformation and Wiener filtering of the projections, Nuclear Instruments and Methods in Physics Research A 423 (1999) 265–271.
- [14] P. Duvauchelle, N. Freud, V. Kaftandjian, D. Babot, A computer code to simulate X-ray imaging techniques, Nuclear Instruments and Methods in Physics Research B 170 (2000) 245–258.
- [15] B. Chalmond, F. Coldefy, B. Lavayssière, Tomographic reconstruction from non-calibrated noisy projections in non-destructive evaluation, Inverse Problems 15 (1999) 399–411.
- [16] NVIDIA CUDA Programming Guide, Version 2.0 <[http://developer.download.nvidia.com/compute/cuda/2.0/docs/NVIDIA\\_CUDA\\_Programming\\_Guide\\_2.0.pdf](http://developer.download.nvidia.com/compute/cuda/2.0/docs/NVIDIA_CUDA_Programming_Guide_2.0.pdf)> (31.01.11).
- [17] Full database of the experimental results <<http://www.inf.u-szeged.hu/~vargalg/research/datasets/projprocessing/index.html>> (31.01.11).
- [18] L. Varga, P. Balázs, A. Nagy, Projection selection algorithms for discrete tomography, Lecture Notes in Computer Science 6474 (2010) 390–401.
- [19] A. Alpers, Instability and Stability in Discrete Tomography, Ph.D. thesis, Technische Universität München, Shaker Verlag, Aachen, 2003.
- [20] B.E. van Dalen, Stability results for two directions in discrete tomography, 2008, arXiv:0804.0316 [math.CO].
- [21] R.J. Gardner, P. Gritzmann, Discrete tomography: determination of finite sets by X-rays, Transactions of the American Mathematical Society 349 (6) (1997) 2271–2295.
- [22] A. Nagy, A. Kuba, Reconstruction of binary matrices from fan-beam projections, Acta Cybernetica 17 (2) (2005) 359–385.
- [23] G. Placidi, M. Alecci, A. Sotgiu, Theory of adaptive acquisition method for image reconstruction from projections and application to EPR imaging, Journal of Magnetic Resonance, Series B (1995) 50–57.